Available online at www.sciencedirect.com
ScienceDirect
Journal of Sound and Vibration 324 (2009) 139–160
JOURNAL OF SOUND AND VIBRATION
www.elsevier.com/locate/jsvi

Modeling and nonlinear hunting stability analysis of high-speed railway vehicle moving on curved tracks

Yung-Chang Cheng[a,*], Sen-Yung Lee[b], Hsing-Hao Chen[a]

[a]*Department of Mechanical and Automation Engineering, National Kaohsiung First University of Science and Technology, Kaohsiung, Taiwan 811, ROC*

[b]*Department of Mechanical Engineering, National Cheng Kung University, Tainan, Taiwan 701, ROC*

Received 25 February 2008; received in revised form 23 January 2009; accepted 27 January 2009
Handling Editor: L.G. Tham
Available online 5 March 2009

Abstract

A heuristic nonlinear creep model is used to derive the nonlinear coupled differential equations of motion of a high-speed railway vehicle traveling on a curved track. The vehicle dynamics are modeled using a 21 degree-of-freedom (21-DOF) system which takes account of the lateral displacement and yaw angle of each wheelset, the lateral displacement, vertical displacement, roll angle and yaw angle of the truck frames, and the lateral displacement, vertical displacement, roll angle, pitch angle and yaw angle of the car body. To analyze the respective effects of the major system parameters on the vehicle dynamics, the 21-DOF system is reduced to 20-DOF, 14-DOF and 6-DOF models, respectively, by excluding designated subsets of the system parameters. The validity of the analytical models and the numerical solution procedure is confirmed by comparing the result obtained using the 6-DOF model for the critical velocity of a railway vehicle traveling on a tangent track with the solution presented in the literature. In general, the results obtained in this study show that the critical hunting speed derived using the 6-DOF or 14-DOF model is generally higher than that evaluated using the 20-DOF model. In addition, the critical hunting speed evaluated via the heuristic nonlinear creep model is lower than that derived using a linear creep model.
© 2009 Elsevier Ltd. All rights reserved.

1. Introduction

With the advent of high-speed passenger trains in many countries around the world, the problem of achieving a comfortable high-speed operation without hunting instability has attracted significant interest in recent years. The literature contains many investigations into the dynamic stability of railway trucks running on curved tracks [1–5]. In these studies, the trucks are generally modeled as a six degree-of-freedom (6-DOF) system, comprising the lateral displacements and yaw angles of the front and rear wheelsets and the truck frame, respectively. In addition, many researchers have applied linear creep models with various DOF to analyze the curving performance and stability of railway vehicles and articulated train sets. For example, Bell et al. [6] studied the curving mechanics and steady-state curving performance of a generic railway vehicle,

*Corresponding author. Tel.: +886 7 6011000 2293; fax: +886 7 6011066.
E-mail address: yccheng@ccms.nkfust.edu.tw (Y.-C. Cheng).

0022-460X/$ - see front matter © 2009 Elsevier Ltd. All rights reserved.
doi:10.1016/j.jsv.2009.01.053

Nomenclature

a half of track gauge
b_1 half of primary yaw spring arm and primary yaw damping arm
b_1 half of primary vertical spring arm and primary vertical damping arm
b_2 half of secondary longitudinal spring arm and secondary vertical spring arm
b_3 half of secondary longitudinal damping arm and secondary vertical damping arm
C_{px} yaw damping of primary suspension
C_{py} lateral damping of primary suspension
C_{pz} vertical damping of primary suspension
C_{sx} yaw damping of secondary suspension
C_{sy} lateral damping of secondary suspension
C_{sz} vertical damping of secondary suspension
f_{11} lateral creep force coefficient
f_{12} lateral/spin creep force coefficient
f_{22} spin creep force coefficient
f_{33} longitudinal creep force coefficient
F_{kxij} linear creep force acting in longitudinal direction on left and right wheels in front and rear wheelsets
F^*_{kxij} linear creep force acting in longitudinal direction on left and right wheels in front and rear wheelsets as computed using Kalker's linear theory
F^n_{kxij} nonlinear creep force acting in x-direction on left and right wheels in front and rear wheelsets
F_{kyij} linear creep force acting in lateral direction on left and right wheels in front and rear wheelsets
F^*_{kyij} linear creep force acting in lateral direction on left and right wheels in front and rear wheelsets as computed using Kalker's linear theory
F^n_{kyij} nonlinear creep force acting in y-direction on left and right wheels in front and rear wheelsets
F_{syc} suspension force acting in lateral direction on half car body
F_{syij} suspension force acting in lateral direction on front and rear wheelsets
F_{syti} suspension force acting in lateral direction on front and rear truck frames
F_{szc} suspension force acting in vertical direction on car body
F_{szti} suspension force acting in vertical direction on front and rear truck frames
h height of external weight above center of gravity of wheelset
h_c vertical distance from wheelset center of gravity to car body
h_T vertical distance from wheelset center of gravity to secondary suspension
$i = 1, 2$ indices denoting front and rear of truck, respectively
I_{cx} roll moment of inertia of car body
I_{cy} pitch moment of inertia of car body
I_{cz} yaw moment of inertia of car body
I_{tx} roll moment of inertia of truck frame
I_{tz} yaw moment of inertia of truck frame
I_{wx} roll moment of inertia of wheelset
I_{wy} spin moment of inertia of wheelset
I_{wz} yaw moment of inertia of wheelset
$j = 1, 2$ indices denoting front and rear wheelsets, respectively
$k = L, R$ indices denoting left and right wheels, respectively
K_{px} longitudinal stiffness of primary suspension
K_{py} lateral stiffness of primary suspension
K_{pz} vertical stiffness of primary suspension
K_{sx} longitudinal stiffness of secondary suspension
K_{sy} lateral stiffness of secondary suspension
K_{sz} vertical stiffness of secondary suspension
L_1 half of primary lateral spring arm
L_2 half of primary lateral damping arm
L_c longitudinal distance from wheelset center of gravity to car body
m_c car body mass
m_t truck frame mass
m_w wheelset mass
M_{kxij} linear creep moment acting in longitudinal direction on left and right wheels in front and rear wheelsets
M_{kzij} linear creep moment acting in vertical direction on left and right wheels in front and rear wheelsets
M^*_{kzij} linear creep moment acting in vertical direction on left and right wheels in front and rear wheelsets as computed using Kalker's linear theory
M^n_{kzij} nonlinear creep moment acting in z-direction on left and right wheels in front and rear wheelsets

M_{sxc}	suspension moment acting in longitudinal direction on car body
M_{sxti}	suspension moment acting in longitudinal direction on front and rear truck frames
M_{syc}	suspension moment acting in lateral direction on car body
M_{szc}	suspension moment acting in vertical direction on car body
M_{szij}	suspension moment acting in vertical direction on front and rear wheelsets
M_{szti}	suspension moment acting in vertical direction on front and rear truck frames
N	normal force acting on wheelset in equilibrium state
N_{Lyij}	normal force acting in lateral direction on left wheel in front and rear wheelsets
N_{Lzij}	normal force acting in vertical direction on left wheel in front and rear wheelsets
N_{Ryij}	normal force acting in lateral direction on right wheel in front and rear wheelsets
N_{Rzij}	normal force acting in vertical direction on right wheel in front and rear wheelsets
r_L	rolling radius of left wheel
r_R	rolling radius of right wheel
r_0	nominal rolling radius of wheelset
R	radius of curvature of track
R_{Lxij}	x component of position vector on left wheel in front and rear wheelsets
R_{Lyij}	y component of position vector on left wheel in front and rear wheelsets
R_{Rxij}	x component of position vector on right wheel in front and rear wheelsets
R_{Ryij}	y component of position vector on right wheel in front and rear wheelsets
t	time
V	forward speed of truck
V_{cr}	critical hunting speed
W	axle load
W_{ext}	external load
x, y, z	longitudinal, lateral and vertical coordinates, respectively
y_c	lateral displacement of car body
y_{ti}	lateral displacement of front and rear truck frames
y_{wij}	lateral displacement of front and rear wheelsets
z_c	vertical displacement of car body
z_{ti}	vertical displacement of front and rear truck frames
α_{ij}	saturation constant in nonlinear creep force model for front and rear wheelsets
β_{ij}	nonlinearity constant in nonlinear creep force model for front and rear wheelsets
β_{kij}	nonlinearity constant in nonlinear creep force model for left and right wheels in front and rear wheelsets
δ_L	contact angle of left wheel
δ_R	contact angle of right wheel
λ	wheel conicity
θ_c	pitch angle of car body
ϕ_c	roll angle of car body
ϕ_{se}	superelevation angle of curved track
ϕ_{ti}	roll angle of front and rear truck frames
ψ_c	yaw angle of car body
ψ_{ti}	yaw angle of front and rear truck frames
ψ_{wij}	yaw angle of front and rear wheelsets

while Ahmed et al. [7] performed computer simulations based on Kalker's linear theory to analyze the curving performance of the French TGV system. Wickens [8] analyzed the curving performance of the vehicle including the unsymmetric truck a symmetric railway vehicle with two unsymmetric two-axle bogies and showed that a perfect steering capability could be achieved by utilizing passive suspension elements in place of conventional linkage systems. However, in Refs. [6–8], the mass of the truck frame was neglected, and thus the dynamic stability of truck system cannot be discussed. Bell and Horak [9] showed that forced-steering railway vehicles have a better curve negotiation capability than conventional and self-steering radial trucks, but experience kinematic instabilities and significantly lower critical speeds for low wheel conicities and creep coefficients, respectively.

In practice, the parameters governing the dynamics of a HSR vehicle are nonlinear rather than linear, and thus the linear creep models utilized in the studies above are liable to a certain degree of error. Zboinski [10,11] presented a series of studies in which he examined the dynamics of a railway vehicle during motion along a curved track utilizing quasi-statistical and dynamical approaches, respectively, and examined the practical significance of considering all the inertial forces when constructing the dynamic equations of motion of a railway vehicle. Zeng and Wu [12] constructed a 17-DOF model of a HSR vehicle and utilized an efficient

numerical method to analyze the critical speed at the Hopf bifurcation point on both straight and curved tracks with various degrees of superelevation. Employing the nonlinear creep model evaluated via the Chartet's equation, Hirotsu et al. [13] derived the nonlinear dynamic equations of motion of a four axle railway vehicle with conventional two axle bogies and performed numerical simulations to examine the vertical and lateral forces acting on the vehicle during curving on rails with lateral irregularities. Zboinski and Dusza [14] examined the nonlinear lateral stability of two-axle and four-axle railway vehicles during curving with particular regard to the effects of the angle of attack, the cant deficiency and excess, and the suspension parameters, respectively.

The nonlinear creep models utilized in Refs. [10–14] neglect the nonlinear creep moments. Moreover, the 6-DOF models in Refs. [1–5] neglect the motion of the car body and assume is mass to coincide with that of the truck frame. In practice, however, the dynamics of a railway vehicle are highly sensitive to the car body motion; particularly when the vehicle is traveling along a curved track. Finally, the 17-DOF model constructed by Zeng and Wu [12] considers the lateral displacement and yaw angle of each wheelset, and the lateral displacements, roll angles and yaw angles of the truck and car body, respectively, but neglects the vertical displacements of the truck frames and the vertical displacement and pitch angle of the car body. Furthermore, while the linear creep models utilized in Refs. [6–9] take into account the effects of the creep force and the creep moment on the critical hunting speed, the effects of the suspension parameters are not considered.

In an attempt to address the various limitations of the linear and nonlinear models discussed above, this study develops a 21-DOF model to analyze the dynamics of a railway vehicle while moving on curved tracks. The model includes the lateral displacement and yaw angle of each wheelset, the lateral displacement, vertical displacement, roll angle and yaw angle of the truck frames, and the lateral displacement, vertical displacement, roll angle, pitch angle and yaw angle of the car body. The nonlinear coupled differential equations of motion of the vehicle are derived using a heuristic nonlinear creep model, while the critical hunting speed is evaluated using the Lyapunov indirect method [15]. To clarify the effects of the major system parameters on the dynamic behavior of the railway vehicle, the 21-DOF model is reduced to a 20-DOF model by excluding the nodding motion (i.e. the pitch angle) of the car body. The 20-DOF model is then further reduced to 14-DOF and 6-DOF models by excluding specified sub-sets of the system parameters (e.g. those relating to the vertical displacements and roll angles of the truck frames and car body, or to the vertical stiffness and vertical damping of the secondary suspension, for example). The validity of the analytical modeling approach and numerical solution procedure is confirmed by comparing the results obtained for the critical speed of a railway vehicle modeled as a 6-DOF system with the results presented in the literature. The results obtained for the critical hunting speed using the proposed nonlinear creep model with various DOFs are then compared and contrasted with those derived using a linear creep model with an equivalent DOF.

2. Differential equations of motion

2.1. Governing equations of motion of truck frame and car body

Consider a railway vehicle moving on a curved track with radius R (see Figs. 1 and 2). The governing equations of motion for the lateral displacement y_{ti}, vertical displacement z_{ti}, roll angle ϕ_{ti} and yaw angle ψ_{ti} of the truck frame are given, respectively, by

$$m_t\ddot{y}_{ti} = F_{syti} + \left(\frac{V^2}{gR} - \phi_{se}\right)m_t g, \tag{1}$$

$$m_t\ddot{z}_{ti} = F_{szti} - \left(1 + \frac{V^2}{gR}\phi_{se}\right)m_t g, \tag{2}$$

$$I_{tx}\ddot{\phi}_{ti} = M_{sxti}, \tag{3}$$

$$I_{tz}\ddot{\psi}_{ti} = M_{szti}. \tag{4}$$

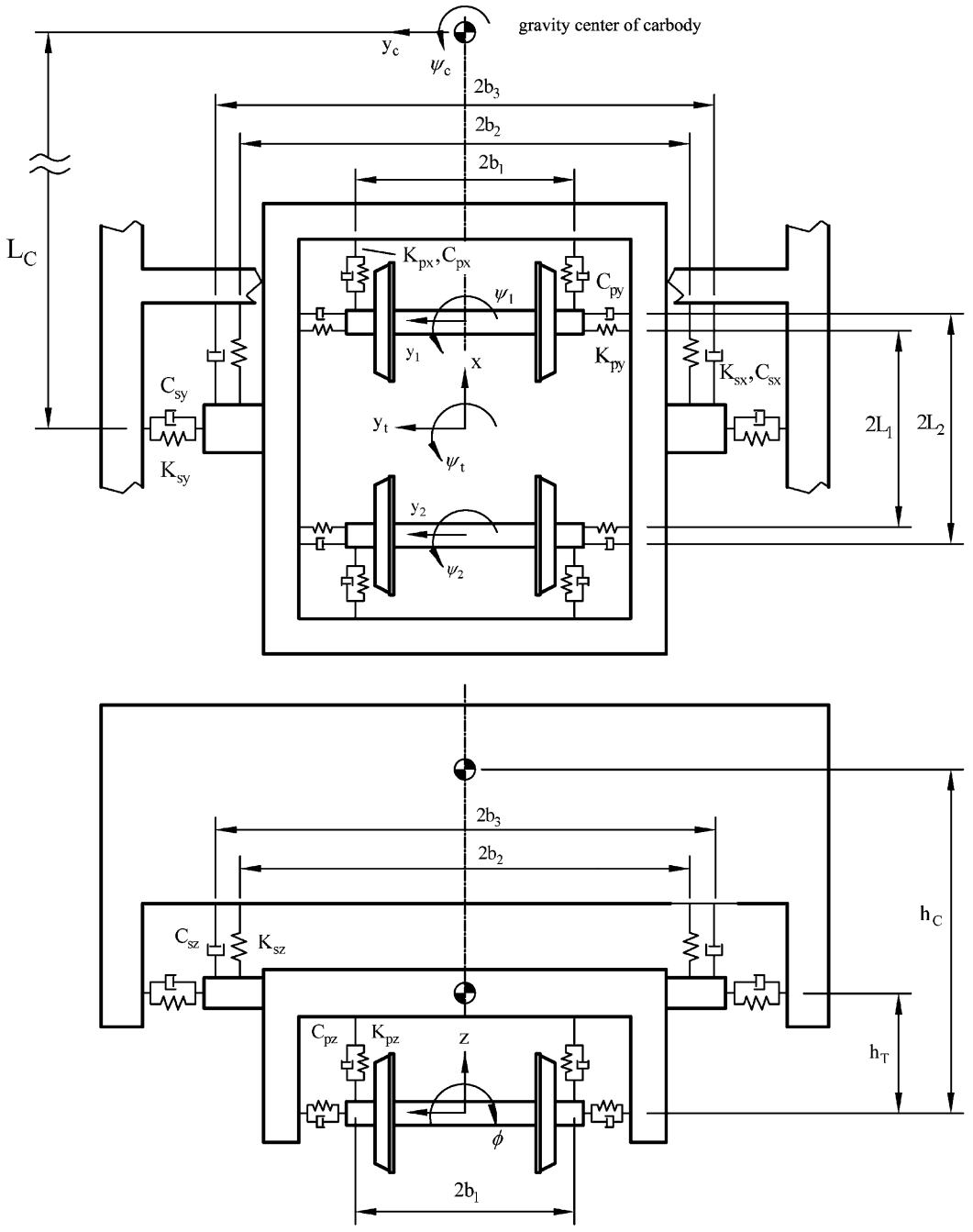

Fig. 1. Car body model.

Meanwhile, the governing equations of motion for the lateral displacement y_c, vertical displacement z_c, pitch angle θ_c, roll angle ϕ_c, and yaw angle ψ_c of the car body are given by

$$m_c\ddot{y}_c = F_{syc} + \left(\frac{V^2}{gR} - \phi_{se}\right)m_c g, \tag{5}$$

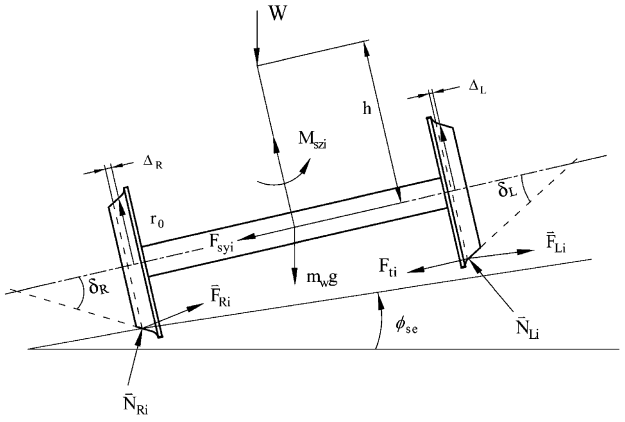

Fig. 2. Free body diagram of single wheelset.

$$m_c\ddot{z}_c = F_{szc} - \left(1 + \frac{V^2}{gR}\phi_{se}\right)m_c g, \tag{6}$$

$$I_{cx}\ddot{\phi}_c = M_{sxc}, \tag{7}$$

$$I_{cy}\ddot{\theta}_c = M_{syc}, \tag{8}$$

$$I_{cz}\ddot{\psi}_c = M_{szc}, \tag{9}$$

where V is the speed of the railway vehicle in the forward direction and ϕ_{se} the superelevation angle of the curved track. Note that subscripts $i = 1, 2$ in Eqs. (1)–(9) indicate that the corresponding physical properties relate to the front and rear of the truck, respectively. Note also that the physical quantities F_{syc}, F_{szc}, F_{syti}, F_{szti}, M_{sxc}, M_{syc}, M_{szc}, M_{sxti} and M_{szti} are defined in the nomenclature. Finally, the double dots above the quantities on the left-hand side of Eqs. (1)–(9) denote differentiation with respect to the time variable t.

2.2. Governing equations of motion of front and rear wheelsets

Applying the notations defined by Dukkipati and Garg [16], and taking the inertia forces and heuristic nonlinear creep forces and moments into consideration, the governing coupled differential equations of motion for the lateral displacement y_{wij} and yaw angle ψ_{wij} of the wheelsets are given by

$$\begin{aligned} m_w\left(\ddot{y}_{wij} - \frac{V^2}{R}\right) = {} & F^n_{Lyij}(y_{wij}, \dot{y}_{wij}, \psi_{wij}, \dot{\psi}_{wij}) + F^n_{Ryij}(y_{wij}, \dot{y}_{wij}, \psi_{wij}, \dot{\psi}_{wij}) \\ & + N_{Lyij} + N_{Ryij} + F_{syij} + \frac{V^2}{gR}W_{ext} - (W_{ext} + m_w g)\phi_{se}, \end{aligned} \tag{10}$$

$$\begin{aligned} I_{wz}\ddot{\psi}_{wij} = {} & -I_{wy}\frac{V}{r_0}\dot{\phi}_{wij} + R_{Rxij}F^n_{Ryij}(y_{wij}, \dot{y}_{wij}, \psi_{wij}, \dot{\psi}_{wij}) - R_{Ryij}F^n_{Rxij}(y_{wij}, \dot{y}_{wij}, \psi_{wij}, \dot{\psi}_{wij}) \\ & + R_{Lxij}F^n_{Lyij}(y_{wij}, \dot{y}_{wij}, \psi_{wij}, \dot{\psi}_{wij}) - R_{Lyij}F^n_{Lxij}(y_{wij}, \dot{y}_{wij}, \psi_{wij}, \dot{\psi}_{wij}) \\ & + (R_{Rxij}N_{Ryij} + R_{Lxij}N_{Lyij}) + M^n_{Lzij}(y_{wij}, \dot{y}_{wij}, \psi_{wij}, \dot{\psi}_{wij}) + M^n_{Rzij}(y_{wij}, \dot{y}_{wij}, \psi_{wij}, \dot{\psi}_{wij}) + M_{szij}, \end{aligned} \tag{11}$$

where the subscripts $j = 1, 2$ indicate that the corresponding properties relate to the front and rear wheelsets, respectively. Furthermore, ϕ_{wij} is the roll angle of the wheelset, and $F^n_{Rxij}(y_{wij}, \dot{y}_{wij}, \psi_{wij}, \dot{\psi}_{wij})$, $F^n_{Ryij}(y_{wij}, \dot{y}_{wij}, \psi_{wij}, \dot{\psi}_{wij})$, $F^n_{Lxij}(y_{wij}, \dot{y}_{wij}, \psi_{wij}, \dot{\psi}_{wij})$ and $F^n_{Lyij}(y_{wij}, \dot{y}_{wij}, \psi_{wij}, \dot{\psi}_{wij})$ are the x- and y-direction

components of the nonlinear creep forces acting on the right and left wheels in the front and rear wheelsets, respectively. Finally, $M^n_{Rzij}(y_{wij}, \dot{y}_{wij}, \psi_{wij}, \dot{\psi}_{wij})$ and $M^n_{Lzij}(y_{wij}, \dot{y}_{wij}, \psi_{wij}, \dot{\psi}_{wij})$ are the nonlinear creep moments acting in the z-direction on the right and left wheels in each wheelset, respectively. Note that the remaining physical parameters, i.e. F_{syij}, M_{szij}, $N_{Lyij}N_{Ryij}$, R_{Lxij}, R_{Lyij}, R_{Rxij} and R_{Ryij}, are fully defined in the nomenclature.

In this study, the dynamics of the railway vehicle are analyzed using a heuristic nonlinear creep model which combines Kalker's linear creep theory [16] with a creep force saturation representation. The nonlinear creep forces in the x- and y-directions and the nonlinear creep moments in the vertical direction are given as (Horak and Wormley [17])

$$F^n_{kxij}(y_{wij}, \dot{y}_{wij}, \psi_{wij}, \dot{\psi}_{wij}) = \alpha_{ij} F_{kxij}, \tag{12a}$$

$$F^n_{kyij}(y_{wij}, \dot{y}_{wij}, \psi_{wij}, \dot{\psi}_{wij}) = \alpha_{ij} F_{kyij}, \tag{12b}$$

$$M^n_{kzij}(y_{wij}, \dot{y}_{wij}, \psi_{wij}, \dot{\psi}_{wij}) = \alpha_{ij} M_{kzij}, \tag{12c}$$

where subscripts $k = L$, R indicate that the corresponding properties relate to the left and right wheels, respectively. Note that the terms F_{kxij}, F_{kyij} and M_{kzij} in Eqs. (12a)–(12c) indicate the linear creep forces and creep moments, respectively.

In the present analysis, an assumption is made that the roll and yaw angles of the two wheelsets are small, and thus the linear creep forces and linear creep moments with respect to the left and right wheels are given by

$$F_{Lxij} = F^*_{Lxij} - F^*_{Lyij}\psi_{wij}, \tag{13a}$$

$$F_{Lyij} = F^*_{Lxij}\psi_{wij} + F^*_{Lyij}, \tag{13b}$$

$$M_{Lzij} = M^*_{Lzij}, \tag{13c}$$

$$F_{Rxij} = F^*_{Rxij} - F^*_{Ryij}\psi_{wij}, \tag{14a}$$

$$F_{Ryij} = F^*_{Rxij}\psi_{wij} + F^*_{Ryij}, \tag{14b}$$

$$M_{Rzij} = M^*_{Rzij}, \tag{14c}$$

where F^*_{kxij}, F^*_{kyij} and M^*_{kyij} are the linear creep forces and linear creep moments given by Kalker's linear theory, and have the forms

$$F^*_{Lxij} = -\frac{f_{33}}{V}\left[V\left(1 + \frac{a}{R} - \frac{r_L}{r_0}\right) - a\dot{\psi}_{wij}\right], \tag{15a}$$

$$F^*_{Lyij} = -\frac{f_{11}}{V}(\dot{y}_{wij} + r_L\dot{\phi}_{wij} - V\psi_{wij}) - \frac{f_{12}}{V}\left(\dot{\psi}_{wij} - \frac{V}{R} - \frac{V}{r_0}\delta_L\right), \tag{15b}$$

$$M^*_{Lzij} = \frac{f_{12}}{V}[\dot{y}_{wij} - V\psi_{wij} + r_L\dot{\phi}_{wij}] - \frac{f_{22}}{V}\left[\dot{\psi}_{wij} - \frac{V}{R} - \frac{V}{r_0}\delta_L\right], \tag{15c}$$

$$F^*_{Rxij} = -\frac{f_{33}}{V}\left[V\left(1 - \frac{a}{R} - \frac{r_R}{r_0}\right) + a\dot{\psi}_{wij}\right], \tag{16a}$$

$$F^*_{Ryij} = -\frac{f_{11}}{V}(\dot{y}_{wij} + r_R\dot{\phi}_{wij} - V\psi_{wij}) - \frac{f_{12}}{V}\left(\dot{\psi}_{wij} - \frac{V}{R} + \frac{V}{r_0}\delta_R\right), \tag{16b}$$

$$M^*_{Rzij} = \frac{f_{12}}{V}[\dot{y}_{wij} - V\psi_{wij} + r_R\dot{\phi}_{wij}] - \frac{f_{12}}{V}\left[\dot{\psi}_{wij} - \frac{V}{R} + \frac{V}{r_0}\delta_R\right]. \tag{16c}$$

The saturation constant α_{ij} in the nonlinear creep formalisms given in Eqs. (12a)–(12c) is defined as (Horak and Wormley [17])

$$\alpha_{ij} = \begin{cases} \dfrac{1}{\beta_{ij}}\left[\beta_{ij} - \dfrac{1}{3}\beta_{ij}^2 + \dfrac{1}{27}\beta_{ij}^3\right] & \text{for } \beta_{ij} \leqslant 3 \\ \dfrac{1}{\beta_{ij}} & \text{for } \beta_{ij} \geqslant 3 \end{cases}, \tag{17}$$

where β_{ij} is nonlinearity constant in the nonlinear creep mode and given by

$$\beta_{ij} = \frac{\beta_{Rij} + \beta_{Lij}}{2} \tag{18}$$

and

$$\beta_{kij} = \frac{\sqrt{(F_{kxij}^*)^2 + (F_{kyij}^*)^2}}{\mu N}. \tag{19}$$

Fig. 3 illustrates the position of the wheelset relative to the curved track. As shown, the contact between the wheel and the track is assumed to be confined to the tread region, i.e. no contact occurs between the left or right wheel flanges and the rail at any point during curving. Assuming that the vehicle remains in a state of static equilibrium as it negotiates the curve, the normal forces acting on the wheelsets in the vertical direction remain constant. Therefore, assuming a simplified truck model with conical wheels, the constant values are taken for Kalker's coefficients [18]. Therefore, the creep coefficients f_{11}, f_{12}, f_{22} and f_{33} in Kalker's linear creep model can also be taken as constants since they vary as a function of the normal force between the wheels and the rails in the vertical direction and the radius of curvature of the wheels at their points of contact with the rails.

Assuming static force equilibrium in the vertical direction, the normal forces acting on the left and right wheels in the vertical direction, i.e. N_{Lzij} and N_{Rzij}, can be obtained as

$$N_{Lzij} = N_{Rzij} = \frac{1}{2}\left(W_{ext} + m_w g + \frac{V^2 W_{ext}}{gR}\phi_{se}\right). \tag{20}$$

Meanwhile, the normal forces acting on the left and right wheels in the lateral direction, i.e. N_{Lyij} and N_{Ryij}, are given as

$$N_{Lyij} = -N_{Lzij}\tan(\delta_L + \phi_{wij}) \approx -\frac{1}{2}\left(W_{ext} + m_w g + \frac{V^2 W_{ext}}{gR}\phi_{se}\right)(\delta_L + \phi_{wij}), \tag{21}$$

$$N_{Ryij} = N_{Rzi}\tan(\delta_R - \phi_{wij}) \approx \frac{1}{2}\left(W_{ext} + m_w g + \frac{V^2 W_{ext}}{gR}\phi_{se}\right)(\delta_R - \phi_{wij}). \tag{22}$$

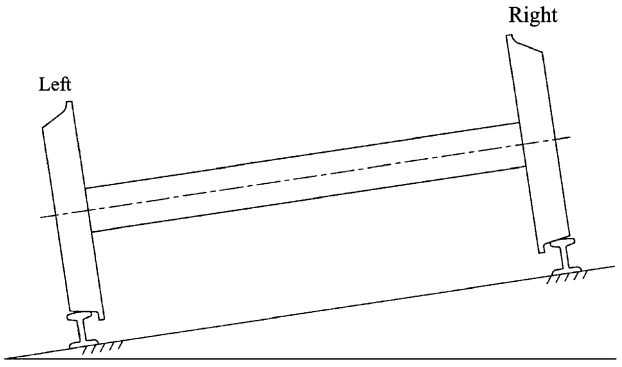

Fig. 3. Position of wheelset relative to track during curving.

Assuming that the lateral displacements Δ_L and Δ_R of the wheel–rail contact points from their equilibrium positions are small, the position vectors of the contact points are given by

$$R_{Rxij} = a\psi_{wij}, \tag{23a}$$

$$R_{Ryij} = -a + r_R\phi_{wij}, \tag{23b}$$

$$R_{Rzij} = -a\phi_{wij} - r_R, \tag{23c}$$

$$R_{Lxij} = -a\psi_{wij}, \tag{23d}$$

$$R_{Lyij} = a + r_L\phi_{wij}, \tag{23e}$$

$$R_{Lzij} = a\phi_{wij} - r_L. \tag{23f}$$

From Eqs. (20)–(23), the normal force in the vertical direction, $R_{Rxij}N_{Ryij} + R_{Lxij}N_{Lyij}$, the summation moments in the longitudinal direction, $R_{Ryij}N_{Rzij} + R_{Lyij}N_{Lzij}$ and $-R_{Rzij}N_{Ryij} - R_{Lzij}N_{Lyij}$, can be obtained.

From Fig. 1, it can be shown that the suspension forces acting on the wheelsets in the lateral direction, F_{syij}, the suspension moments acting on the wheelsets in the vertical direction, M_{szij}, the suspension forces acting on the truck frames in the lateral direction, F_{syti}, the suspension forces acting on the truck frames in the vertical direction F_{szti}, the suspension moments acting on the truck frames in the longitudinal direction, M_{sxti}, and the suspension moments acting on the truck frames in the vertical direction, M_{szti}, are given, respectively, as follows:

$$\begin{aligned} F_{syij} = & -2K_{py}y_{wij} - (-1)^j 2K_{py}L_1\psi_{ti} + 2K_{py}y_{ti} - 2C_{py}\dot{y}_{wij} - (-1)^j 2C_{py}L_2\dot{\psi}_{ti} \\ & + 2C_{py}\dot{y}_{ti} + 2K_{py}h_T\phi_{ti} + 2C_{py}h_T\dot{\phi}_{ti}, \end{aligned} \tag{24}$$

$$M_{szij} = 2K_{px}b_1^2\psi_{ti} + 2C_{px}b_1^2\dot{\psi}_{ti} - 2K_{px}b_1^2\psi_{wij} - 2C_{px}b_1^2\dot{\psi}_{wij}, \tag{25}$$

$$\begin{aligned} F_{syti} = & 2K_{py}y_{wij} + 2C_{py}\dot{y}_{wij} + (-4K_{py} - 2K_{sy})y_{ti} + (-4C_{py} - 2C_{sy})\dot{y}_{ti} + 2K_{sy}L_c\psi_c + 2C_{sy}L_c\dot{\psi}_c \\ & + 2K_{sy}y_c + 2C_{sy}\dot{y}_c + 2K_{sy}(h_c - h_T)\phi_c + 2C_{sy}(h_c - h_T)\dot{\phi}_c - 4K_{py}h_T\phi_{ti} - 4C_{py}h_T\dot{\phi}_{ti}, \end{aligned} \tag{26}$$

$$F_{szti} = 2K_{sz}z_c + 2C_{sz}\dot{z}_c - 2(K_{sz} + 2K_{pz})z_{ti} - 2(C_{sz} + 2C_{pz})\dot{z}_{ti}, \tag{27}$$

$$\begin{aligned} M_{sxti} = & 2K_{sz}b_2^2\phi_c + 2C_{sz}b_3^2\dot{\phi}_c - 2K_{sz}b_2^2\phi_{ti} - 2C_{sz}b_3^2\dot{\phi}_{ti} + \left[2K_{py}h_T + 2K_{pz}b_1^2\left(\frac{\lambda}{a}\right)\right]y_{wij} - 4K_{py}h_Ty_{ti} \\ & + \left[2C_{py}h_T + 2C_{pz}b_1^2\left(\frac{\lambda}{a}\right)\right]\dot{y}_{wij} - 4C_{py}h_T\dot{y}_{ti} - 4K_{py}h_T^2\phi_{ti} - 4C_{py}h_T^2\dot{\phi}_{ti} - 4K_{pz}b_1^2\phi_{ti} - 4C_{pz}b_1^2\dot{\phi}_{ti}, \end{aligned} \tag{28}$$

$$\begin{aligned} M_{szti} = & (-4K_{py}L_1^2 - 4K_{px}b_1^2 - 2K_{sx}b_2^2)\psi_{ti} + (-4C_{py}L_2^2 - 4C_{px}b_1^2 - 2C_{sx}b_3^2)\dot{\psi}_{ti} \\ & + 2K_{py}L_1y_{wi1} + 2C_{py}L_2\dot{y}_{wi1} + 2K_{px}b_1^2\psi_{wi1} + 2C_{px}b_1^2\dot{\psi}_{wi1} - 2K_{py}L_1y_{wi2} - 2C_{py}L_2\dot{y}_{wi2} \\ & + 2K_{px}b_1^2\psi_{wi2} + 2C_{px}b_1^2\dot{\psi}_{wi2} + 2K_{sx}b_2^2\psi_c + 2C_{sx}b_3^2\dot{\psi}_c. \end{aligned} \tag{29}$$

Meanwhile, regarding the car body, the suspension forces acting in the lateral direction, F_{syc}, the suspension forces acting in the vertical direction, F_{szc}, the suspension moments acting in the longitudinal direction, M_{sxc}, the suspension moments acting in the lateral direction, M_{syc}, and the suspension moments acting in the vertical direction, M_{szc}, are given as

$$F_{syc} = -2K_{sy}(2y_c - y_{t1} - y_{t2}) - 4K_{sy}(h_c - h_T)\phi_c - 2C_{sy}(2\dot{y}_c - \dot{y}_{t1} - \dot{y}_{t2}) - 4C_{sy}(h_c - h_T)\dot{\phi}_c, \tag{30}$$

$$F_{szc} = -4K_{sz}z_c - 4C_{sz}\dot{z}_c + 2K_{sz}z_{t1} + 2C_{sz}\dot{z}_{t1} + 2K_{sz}z_{t2} + 2C_{sz}\dot{z}_{t2}, \tag{31}$$

$$\begin{aligned}M_{sxc} = {} & 2K_{sz}b_2^2\phi_{t1} + 2C_{sz}b_3^2\dot{\phi}_{t1} + 2K_{sz}b_2^2\phi_{t2} + 2C_{sz}b_3^2\dot{\phi}_{t2} - 4K_{sz}b_2^2\phi_c - 4C_{sz}b_3^2\dot{\phi}_c \\ & - 4K_{sy}(h_c - h_T)y_c - 4C_{sy}(h_c - h_T)\dot{y}_c + 2K_{sy}(h_c - h_T)y_{t1} + 2C_{sy}(h_c - h_T)\dot{y}_{t1} \\ & + 2K_{sy}(h_c - h_T)y_{t2} + 2C_{sy}(h_c - h_T)\dot{y}_{t2} - 4K_{sy}(h_c - h_T)^2\phi_c - 4C_{sy}(h_c - h_T)^2\dot{\phi}_c \\ & - 4K_{sy}(h_c - h_T)L_c\psi_c - 4C_{sy}(h_c - h_T)L_c\dot{\psi}_c, \end{aligned} \tag{32}$$

$$M_{syc} = -2K_{sz}z_{t1} + 2K_{sz}z_{t2} - 4K_{sz}\theta_c L_c - 2C_{sz}\dot{z}_{t1} + 2C_{sz}\dot{z}_{t2} - 4C_{sz}\dot{\theta}_c L_c, \tag{33}$$

$$\begin{aligned}M_{szc} = {} & -4K_{sy}\psi_c L_c^2 - 4C_{sy}\dot{\psi}_c L_c^2 - 2K_{sx}b_2^2(2\psi_c - \psi_{t1} - \psi_{t2}) \\ & - 2C_{sx}b_3^2(2\dot{\psi}_c - \dot{\psi}_{t1} - \dot{\psi}_{t2}) - 2K_{sy}L_c(-y_{t1} - y_{t2}) - 2C_{sy}L_c(-\dot{y}_{t1} - \dot{y}_{t2}). \end{aligned} \tag{34}$$

For simplicity, it is assumed that the constraint function is linear for a conical wheel on a knife-edged rail. Hence, the following assumptions regarding the wheel–rail geometry can be employed:

$$\delta_L = \delta_R = \lambda, \quad \tfrac{1}{2}(r_L - r_R) = \lambda y_{wij}, \quad \tfrac{1}{2}(r_L + r_R) = r_0. \tag{35}$$

Substituting Eqs. (12)–(23), (35) into Eqs. (10) and (11) and neglecting the higher order terms and the influence of the vertical displacement of the wheelset axle in the midpoint position on the lateral displacements of the left and right wheels, the following coupled nonlinear differential equations are obtained

$$\begin{aligned}m_w\left(\ddot{y}_{wij} - \frac{V^2}{R}\right) = {} & -\frac{2\alpha_{ij}f_{11}}{V}(\dot{y}_{wij} - V\psi_{wij}) - \frac{2\alpha_{ij}f_{12}}{V}\left(\dot{\psi}_{wij} - \frac{V}{R}\right) - \frac{2r_0\alpha_{ij}f_{11}}{V}\left(\frac{\lambda}{a}\right)\dot{y}_{wij} \\ & - \left(W_{ext} + m_w g + \frac{V^2 W_{ext}}{gR}\phi_{se}\right)\left(\frac{\lambda}{a}\right)y_{wij} - (W_{ext} + m_w g)\phi_{se} + \frac{V^2 W_{ext}}{gR} + F_{syij}, \end{aligned} \tag{36}$$

$$\begin{aligned}I_{wz}\ddot{\psi}_{wij} = {} & -\frac{2a\lambda\alpha_{ij}f_{33}}{r_o}y_{wij} + \frac{2\alpha_{ij}f_{12}}{V}\dot{y}_{wij} - \left(I_{wy}\frac{V}{r_o} - \frac{2r_o\alpha_{ij}f_{12}}{V}\right)\left(\frac{\lambda}{a}\right)\dot{y}_{wij} - 2\alpha_{ij}f_{12}\psi_{wij} \\ & + \left(W_{ext} + m_w g + \frac{V^2 W_{ext}}{gR}\phi_{se}\right)a\lambda\psi_{wij} + M_{szij} - \left(\frac{2a^2\alpha_{ij}f_{33}}{V} + \frac{2\alpha_{ij}f_{22}}{V}\right)\dot{\psi}_{wij} + \frac{2\alpha_{ij}}{R}(a^2 f_{33} + f_{22}). \end{aligned} \tag{37}$$

where $\alpha_{ij} = \alpha_{ij}(y_{wij}, \dot{y}_{wij}, \psi_{wij}, \dot{\psi}_{wij})$. The 21-DOF model of the railway vehicle is therefore given by Eqs. (1)–(9) and (36)–(37).

2.3. Limiting studies

When $\alpha_{ij} = 1$, the heuristic nonlinear creep model given in Eq. (12) reduces to a linear creep model and the nonlinear differential equations given in Eqs. (36) and (37) reduce to the governing differential equations of motion of a wheelset moving on a curved track based on a linear creep model, i.e.

$$\begin{aligned}m_w\left(\ddot{y}_{wij} - \frac{V^2}{R}\right) = {} & -\frac{2f_{11}}{V}(\dot{y}_{wij} - V\psi_{wij}) - \frac{2f_{12}}{V}\left(\dot{\psi}_{wij} - \frac{V}{R}\right) - \frac{2r_0 f_{11}}{V}\left(\frac{\lambda}{a}\right)\dot{y}_{wij} \\ & - \left(W_{ext} + m_w g + \frac{V^2 W_{ext}}{gR}\phi_{se}\right)\left(\frac{\lambda}{a}\right)y_{wij} - (W_{ext} + m_w g)\phi_{se} + \frac{V^2 W_{ext}}{gR} + F_{syij}, \end{aligned} \tag{38}$$

$$\begin{aligned}I_{wz}\ddot{\psi}_{wij} = {} & -\frac{2a\lambda f_{33}}{r_o}y_{wij} + \frac{2f_{12}}{V}\dot{y}_{wij} - \left(I_{wy}\frac{V}{r_o} - \frac{2r_o f_{12}}{V}\right)\left(\frac{\lambda}{a}\right)\dot{y}_{wij} - 2f_{12}\psi_{wij} \\ & + \left(W_{ext} + m_w g + \frac{V^2 W_{ext}}{gR}\phi_{se}\right)a\lambda\psi_{wij} + M_{szij} - \left(\frac{2a^2 f_{33}}{V} + \frac{2f_{22}}{V}\right)\dot{\psi}_{wij} + \frac{2}{R}(a^2 f_{33} + f_{22}). \end{aligned} \tag{39}$$

Eqs. (1)–(9), (38) and (39) therefore represent the 21-DOF linear creep model of the railway vehicle while traveling on a curved track. In analyzing the hunting stability of the railway vehicle, this study neglects the nodding motion (i.e. the pitch angle) of the car body. The resulting 20-DOF nonlinear creep model for the

railway vehicle is therefore given by Eqs. (1)–(7), (9), (36) and (37), while the equivalent linear creep model is given by Eqs. (1)–(7), (9), (38) and (39).

In addition, neglecting the lateral displacement, vertical displacement, roll angle and yaw angle of the car body, and the vertical displacement and roll angle of the truck frame, and assigning parameter values of $\phi_{wij} = \lambda y_{wij}/a$, $\phi_{se} = 0$, $W = W_{ext} + m_w g$ and $R = \infty$, the nonlinear differential equations given above can be further reduced to the governing differential equations of motion for wheelsets moving on tangent tracks based on a linear creep model, i.e.

$$\begin{aligned} m_w \ddot{y}_{wi} = & -\frac{2f_{11}}{V}\dot{y}_{wi} + 2f_{11}\psi_{wi} - \frac{2f_{12}}{V}\dot{\psi}_{wi} - W\frac{\lambda}{a}y_{wi} - \frac{2r_o f_{11}}{V}\left(\frac{\lambda}{a}\right)\dot{y}_{wi} \\ & - 2K_{py}y_{wi} - (-1)^i 2K_{py}L_1\psi_t + 2K_{py}y_t - 2C_{py}\dot{y}_{wi} - (-1)^i 2C_{py}L_2\dot{\psi}_t + 2C_{py}\dot{y}_t, \end{aligned} \tag{40}$$

$$\begin{aligned} I_{wz}\ddot{\psi}_{wi} = & -\frac{2af_{33}\lambda}{r_o}y_{wi} + \frac{2f_{12}}{V}\dot{y}_{wi} + (-2f_{12} + a\lambda W)\psi_{wi} + \left(-\frac{2a^2 f_{33}}{V} - \frac{2f_{22}}{V}\right)\dot{\psi}_{wi} \\ & + \left[-\frac{I_{wy}V}{r_o} + \frac{2r_o f_{12}}{V}\right]\left(\frac{\lambda}{a}\right)\dot{y}_{wi} + M_{szi}. \end{aligned} \tag{41}$$

Furthermore, the differential equation of motion in the lateral direction for the truck frame moving on tangent tracks simplifies to the following:

$$m_t\ddot{y}_t = 2K_{py}y_{w1} + 2C_{py}\dot{y}_{w1} + 2K_{py}y_{w2} + 2C_{py}\dot{y}_{w2} + (-4K_{py} - 2K_{sy})y_t + (-4C_{py} - 2C_{sy})\dot{y}_t. \tag{42}$$

Eqs. (4) and (40)–(42) represent the 6-DOF model of the railway vehicle dynamics and are identical to those given by Ahmadian and Yang [19].

3. Stability analysis

In this paper, the effects of the various physical parameters on the critical hunting speed of the railway vehicle are analyzed using the Lyapunov indirect method (Vidyasager [15]) Thus, the 20-DOF nonlinear creep model for the railway vehicle given in Eqs. (1)–(7), (9), (36) and (37) can be re-expressed as the following system of first-order differential equations:

$$\dot{\mathbf{x}}(\mathrm{t}) = \mathbf{f}[\mathbf{x}(t)], \tag{43}$$

where $\mathbf{x}(t)$ is a 40×1 vector of the state variables.

For any given vehicle velocity, V, the following determinant matrix can be defined:

$$\mathbf{A} = \left[\frac{\partial \mathbf{f}(\mathbf{x})}{\partial \mathbf{x}}\right]_{\mathbf{x}=\mathbf{x_0}}, \tag{44}$$

where $\mathbf{x_0}$ is the equilibrium point and satisfies $\mathbf{f}[\mathbf{x_0}] = \mathbf{0}$. With the matrix theory in linear algebra, Matrix $\mathbf{A}$ has 40 eigenvalues. The stability conditions of the dynamic railway vehicle can be evaluated by determining whether the eigenvalues of Matrix $\mathbf{A}$ lie on the real or imaginary planes, respectively. If the vehicle velocity V is low, all the eigenvalues will be located in the left half-plane, indicating that the system is stable. However, when V is increased, if any of the eigenvalues are located on the imaginary axis, the dynamic system is judged to be unstable. In other words, the dynamic system is regarded as unstable if any of the eigenvalues of matrix $\mathbf{A}$ have a positive real part. In the present study, the problem of determining the maximum allowable velocity of the railway vehicle (i.e. the critical hunting speed, V_{cr}) is solved as follows: First, an initial vehicle speed V is assigned. Then, the equilibrium point $\mathbf{x_0}$ is found by using Newton's root finding method to determine the root of $\mathbf{f}[\mathbf{x}] = \mathbf{0}$. The equilibrium point $\mathbf{x_0}$ is then substituted into Eq. (44) and matrix $\mathbf{A}$ is constructed. The eigenvalues of matrix $\mathbf{A}$ are then obtained. The stability or otherwise of the railway vehicle at the specified value of the forward velocity, V, is then determined by examining the sign of the real part of each eigenvalue. Assuming that the system is found to be stable, the velocity is increased and the solution procedure is repeated. This process is repeated iteratively until the sign of one of the eigenvalues of matrix $\mathbf{A}$ is found to have a non-positive real part. The corresponding value of V is then taken as the critical hunting speed of the vehicle.

4. Numerical results

To confirm the validity of the analytical models developed in Section 2 and the numerical method presented in Section 3, the critical hunting speed of a railway vehicle was compared with the equivalent solution presented by Ahmadian and Yang [19]. Note that the vehicle was assumed to travel on a tangent track and its dynamics were modeled using the reduced 6-DOF model presented in Section 2.3. The critical hunting speed was determined to be 118 km/h, i.e. identical to that presented in Ref. [19]. Thus, the validity of the proposed approach was confirmed.

As discussed in Section 2.3, in analyzing the hunting stability of the railway vehicle, the current analysis neglects the pitch angle motion of the car body. Therefore, the full 21-DOF model of the vehicle dynamics is reduced to a 20-DOF model. In addition, a simplified 6-DOF model is obtained by neglecting the lateral displacement, vertical displacement, roll angle and yaw angle of the car body, and the vertical displacement and roll angle of the truck frame (see Section 2.3). Finally, a 14-DOF model is constructed by removing the bounce and roll motions of the truck and car body from the 20-DOF model. Compared to the 6-DOF and 14-DOF models, the 20-DOF model includes the vertical stiffness and vertical damping properties of the secondary suspension. Thus, the 20-DOF model allows useful insights to be obtained into the respective effects of these parameters on the dynamics of the railway vehicle on a curved track, and therefore addresses a perceived lack in the present literature. (Note that the contents of each of the DOF models are summarized in

Table 1
Components of each DOF model.

Vehicle system	Lateral displacement	Vertical displacement	Roll angle	Pitch angle	Yaw angle
6 DOF	y_{wi}, y_t				ψ_{wi}, ψ_t
14 DOF	y_{wij}, y_{ti}, y_c				ψ_{wij}, ψ_{ti}, ψ_c
20 DOF	y_{wij}, y_{ti}, y_c	z_{ti}, z_c	ϕ_{ti}, ϕ_c		ψ_{wij}, ψ_{ti}, ψ_c
21 DOF	y_{wij}, y_{ti}, y_c	z_{ti}, z_c	ϕ_{ti}, ϕ_c	θ_c	ψ_{wij}, ψ_{ti}, ψ_c

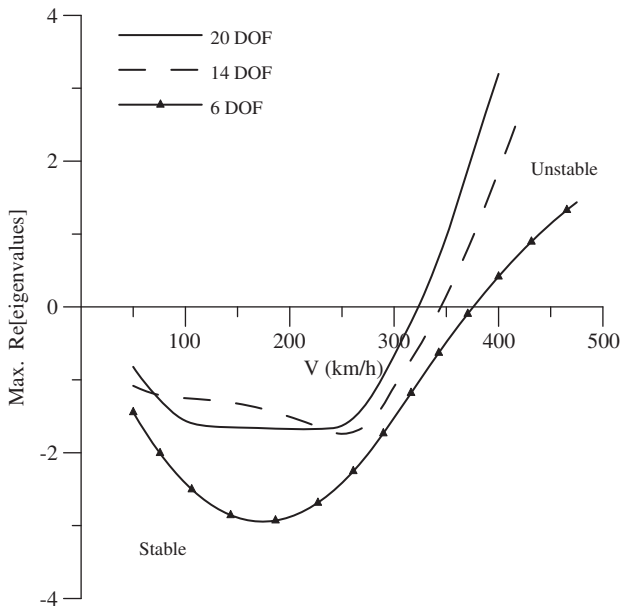

Fig. 4. The relation between the speed and the maximum real part of the eigenvalues at the equilibrium point with respect to the various degrees of freedom systems.

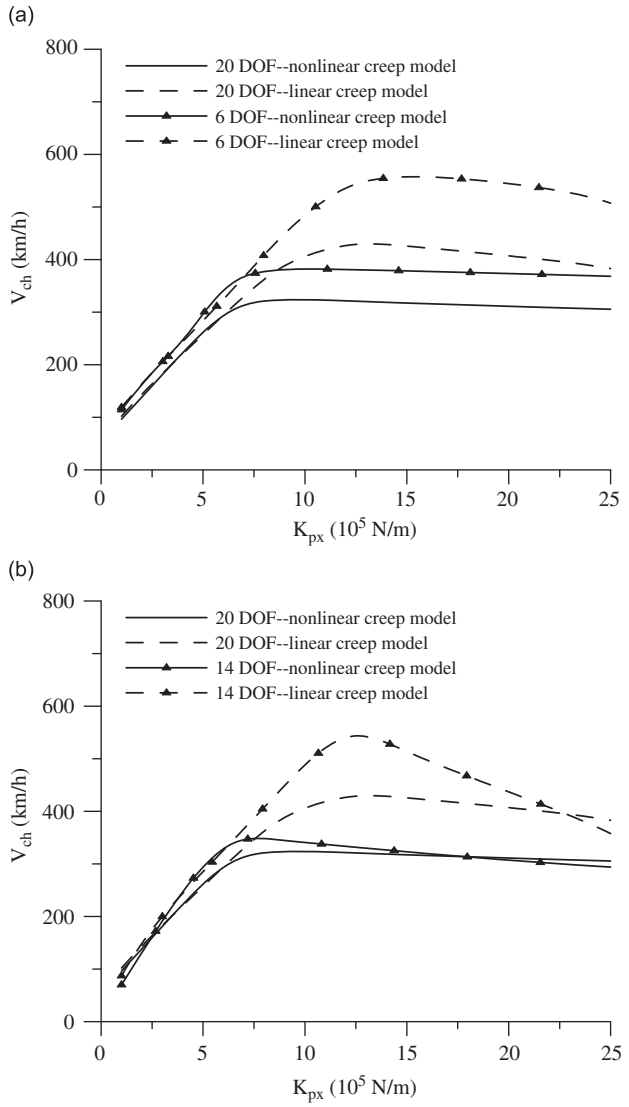

Fig. 5. Influence of longitudinal stiffness of primary suspension K_{px} on critical speed of railway vehicle moving on curved tracks as evaluated using linear and nonlinear creep models with various degrees of freedom ($K_{py} = 3.9 \times 10^5$ N/m, $C_{sx} = 6 \times 10^4$ N s/m, $K_{sx} = 3.5 \times 10^4$ N/m, $C_{sz} = 4 \times 10^4$ N s/m, $K_{sz} = 3.5 \times 10^5$ N/m, $R = 6250$ m).

Table 1.) In performing the following analyses, the various system parameters are assigned the values shown in Appendix A (derived from Refs. [20,21]) unless stated otherwise.

From Fig. 4, one can observe that for each given speed, it corresponds to only one value of the maximum real part of the eigenvalues at the equilibrium point. The critical hunting speed can be obtained when the property of the maximum real part changes from negative to positive. Moreover, the system will be stable if the maximum real part of the eigenvalues is negative. Therefore, the margin of stability for the 6-DOF, 14-DOF and 20-DOF systems can be found.

Figs. 5(a) and (b) illustrate the influence of the longitudinal stiffness of the primary suspension K_{px} on the critical hunting speed of the railway vehicle when moving on a curved track. Note that the results are evaluated using both linear and nonlinear creep models with 6-, 14- and 20-DOF, respectively. In general, it is seen that the critical hunting speed first increases and then decreases as the value of K_{px} is increased. Furthermore, in both figures, it is observed that the critical hunting speeds obtained using the linear creep

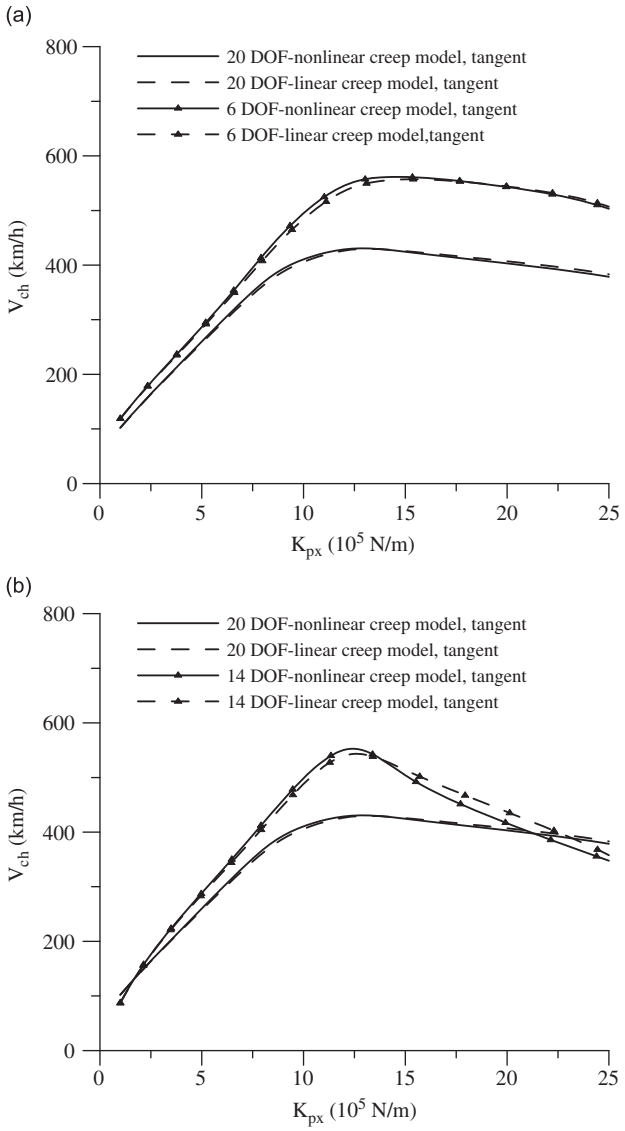

Fig. 6. Influence of longitudinal stiffness of primary suspension K_{px} on critical speed of railway vehicle moving on tangent tracks as evaluated using linear and nonlinear creep models with various degrees of freedom ($K_{py} = 3.9 \times 10^5$ N/m, $C_{sx} = 6 \times 10^4$ N s/m, $K_{sx} = 3.5 \times 10^4$ N/m, $C_{sz} = 4 \times 10^4$ N s/m, $K_{sz} = 3.5 \times 10^5$ N/m, tangent tracks).

model are higher than those evaluated using the nonlinear creep model with an equivalent DOF. In Fig. 5(a), it can be seen that for both the linear and the nonlinear creep models, the critical hunting speeds obtained using the 6-DOF system are greater than those obtained using the 20-DOF system at all values of K_{px}. Fig. 5(b) shows that the critical hunting speeds obtained using the 14-DOF system are higher than those obtained from the 20-DOF system for most values of K_{px} for both creep models. However, at higher values of K_{px}, the critical hunting speeds obtained using the 20-DOF system are higher than those obtained using the 14-DOF system.

The difference in value of the critical hunting speeds obtained using the linear and nonlinear creep models, respectively, reflects the differing assumptions made in Kalker's linear creep model [16] and the current heuristic nonlinear creep model. For example, in Kalker's linear model, it is assumed that for very small creepages, the area of slip is so small that its influence can be neglected, and hence the adhesion zone is

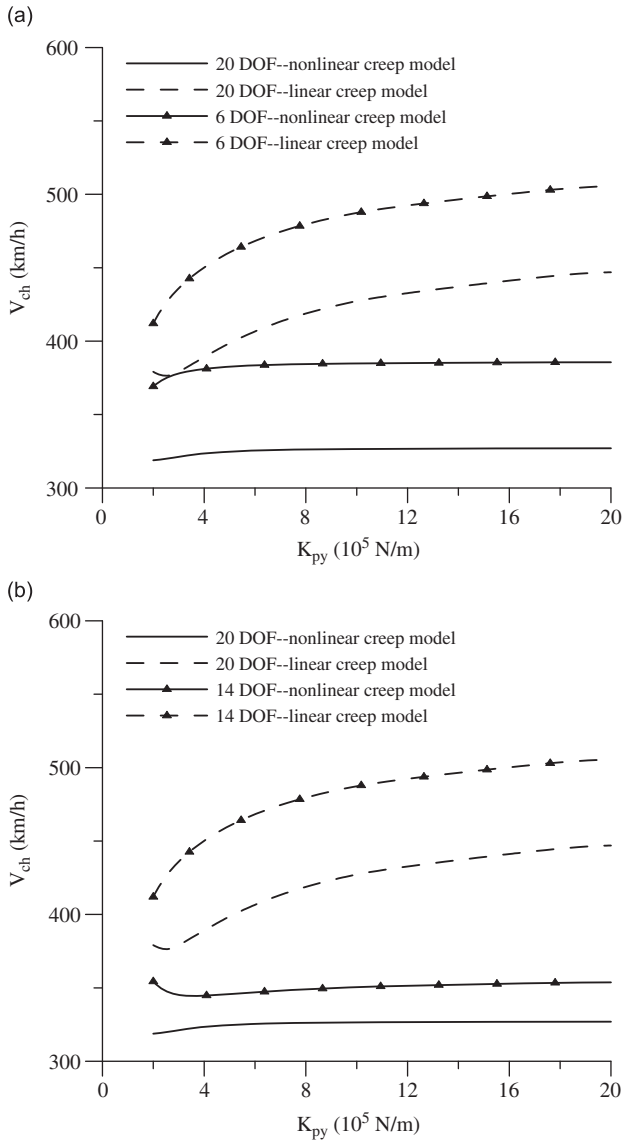

Fig. 7. Influence of lateral stiffness of primary suspension K_{py} on critical speed of railway vehicle as evaluated using linear and nonlinear creep models with various degrees of freedom ($K_{px} = 9 \times 10^5$ N/m, $C_{sx} = 6 \times 10^4$ N s/m, $K_{sx} = 3.5 \times 10^4$ N/m, $C_{sz} = 4 \times 10^4$ N s/m, $K_{sz} = 3.5 \times 10^5$ N/m, $R = 6250$ m).

assumed to cover the entire area of contact. However, the heuristic nonlinear creep model is based on Johnson and Vermeulen's theory [16] which states that the contact area is actually divided into two regions, namely the slip region and the adhesion region. The occurrence of slip in the contact area reduces the forward velocity of the vehicle, and thus the critical hunting speeds determined using the heuristic nonlinear creep model are generally lower than those evaluated using the linear creep model.

Fig. 6 shows the influence of the longitudinal stiffness of the primary suspension K_{px} on the critical hunting speed of the railway vehicle while traveling on tangent tracks. Note that the results are once again obtained using linear and nonlinear creep models with 6-, 14- or 20-DOF, respectively. Fig. 6(a) shows that in the 20-DOF and 6-DOF systems, the critical hunting speeds obtained using the linear creep model are virtually identical to those obtained using the nonlinear model. Moreover, it is evident that the critical hunting speeds obtained from the 20-DOF model are lower than those obtained from the 6-DOF model at all values of K_{px}.

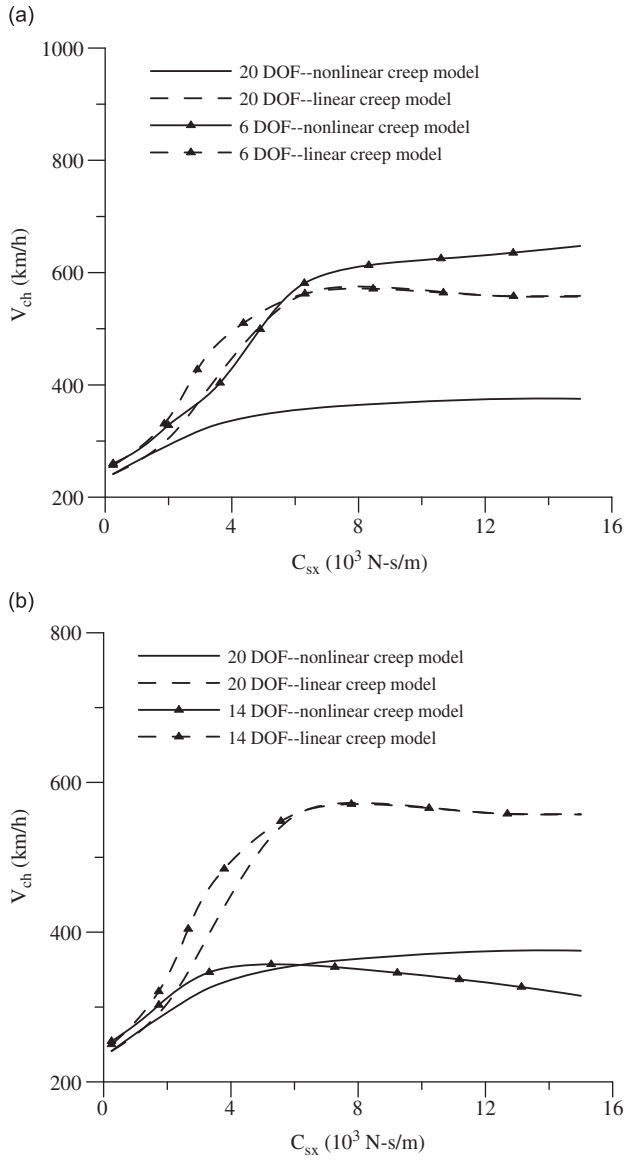

Fig. 8. Influence of longitudinal damping of secondary suspension C_{sx} on critical speed of railway vehicle as evaluated using linear and nonlinear creep models with various degrees of freedom ($K_{px} = 9 \times 10^5$ N/m, $K_{py} = 3.9 \times 10^5$ N/m, $K_{sx} = 3.5 \times 10^4$ N/m, $C_{sz} = 4 \times 10^4$ N s/m, $K_{sz} = 3.5 \times 10^5$ N/m, $R = 6250$ m).

Fig. 6(b) shows that when the vehicle dynamics are modeled as a 14-DOF system, the critical hunting speeds evaluated by the linear creep model are noticeably higher than those obtained from the nonlinear creep model when K_{px} increases beyond a certain critical value. In addition, at values of K_{px} greater than 21×10^5 N/m, the critical hunting speeds evaluated using the 20-DOF creep models are higher than those obtained from the 14-DOF models.

Fig. 7 shows the influence of the lateral stiffness of the primary suspension, K_{py}, on the critical hunting speed of the railway wheel when moving on a curved track. In general, the results show that irrespective of the creep model applied or the number of DOF used to model the vehicle dynamics, the critical speed increases with an increasing value of K_{py}. In addition, the critical hunting speeds evaluated by the linear creep model are consistently higher than those evaluated by the nonlinear creep model. Finally, for both creep models, the

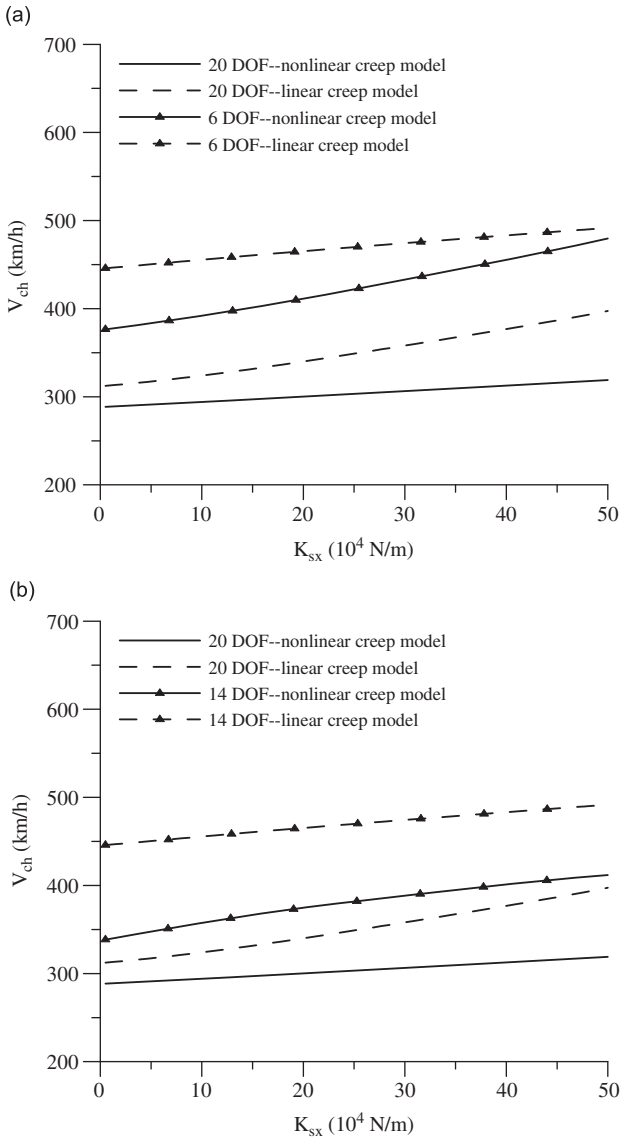

Fig. 9. Influence of longitudinal stiffness of secondary suspension K_{sx} on critical speed of railway vehicle as evaluated using linear and nonlinear creep models with various degrees of freedom ($K_{px} = 9 \times 10^5$ N/m, $K_{py} = 3.9 \times 10^5$ N/m, $C_{sx} = 6 \times 10^4$ N s/m, $C_{sz} = 4 \times 10^4$ N s/m, $K_{sz} = 3.5 \times 10^5$ N/m, $R = 6250$ m).

critical hunting speeds obtained from the 6-DOF and 14-DOF systems are higher than those obtained from the 20-DOF system.

Fig. 8 illustrates the effect of the longitudinal damping of the secondary suspension, C_{sx}, on the critical hunting speed of the railway vehicle. In general, it is noted that the critical speed increases as the longitudinal damping is increased. Fig. 8(a) shows that in the case of the nonlinear creep model, the critical hunting speeds evaluated by the 6-DOF model are consistently higher than those obtained using the 20-DOF model. However, for the linear creep model, little difference exists in the critical hunting speeds obtained from the 6-DOF and 20-DOF systems, respectively, when C_{sx} exceeds a critical value of approximately 5×10^3 N s/m. In addition, when modeling the vehicle dynamics using a 20-DOF system, the critical hunting speeds obtained using the linear creep model are consistently higher than those obtained from the nonlinear model. However, for the 6-DOF system, the critical hunting speeds evaluated using the nonlinear

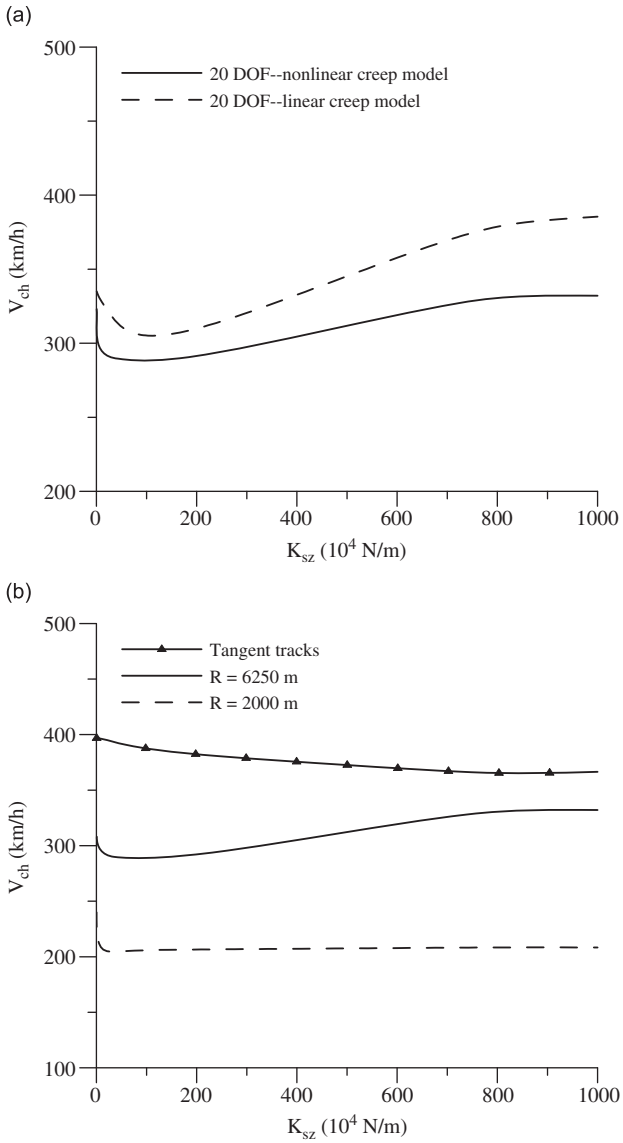

Fig. 10. Influence of vertical stiffness of secondary suspension K_{sz} on critical speed of railway vehicle as evaluated using: (a) 20-DOF linear and nonlinear creep models and (b) 20-DOF nonlinear creep model for tracks with various radii ($K_{px} = 9 \times 10^5$ N/m, $K_{py} = 3.9 \times 10^5$ N/m, $C_{sx} = 6 \times 10^4$ N s/m, $K_{sx} = 3.5 \times 10^4$ N/m, $C_{sz} = 4 \times 10^4$ N s/m).

creep model exceed those obtained from the linear model at values of C_{sx} greater than around 5×10^3 N s/m. Referring to Fig. 8(b), it is seen that in the nonlinear analysis, the critical hunting speed evaluated using the 20-DOF model is higher than that obtained from the 14-DOF model at all values of C_{sx} greater than 6×10^3 N s/m. However, in the case of the linear creep model, the critical hunting speeds obtained using the 14-DOF and 20-DOF models are virtually identical at values of C_{sx} in excess of 7×10^3 N s/m. Finally, when the vehicle dynamics are modeled using the 14-DOF system, the results obtained for the critical hunting speed using the linear creep model are consistently higher than those obtained from the nonlinear creep model.

Fig. 9 illustrates the effect of the longitudinal stiffness of the secondary suspension, K_{sx}, on the critical hunting speed, as evaluated using both the linear and the nonlinear creep models with 6, 14 and 20 DOF,

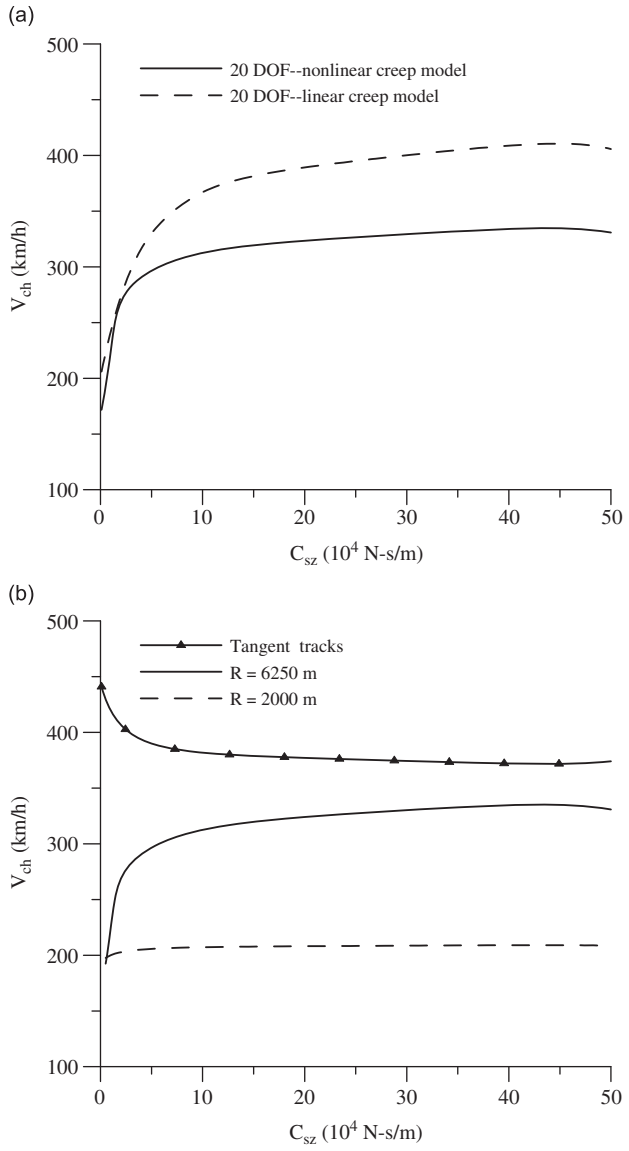

Fig. 11. Influence of vertical damping of secondary suspension C_{sz} on critical speed of railway vehicle as evaluated using: (a) 20-DOF linear and nonlinear creep models and (b) 20-DOF nonlinear creep model for tracks with various radii ($K_{px} = 9 \times 10^5$ N/m, $K_{py} = 3.9 \times 10^5$ N/m, $C_{sx} = 6 \times 10^4$ N s/m, $K_{sx} = 3.5 \times 10^4$ N/m, $K_{sz} = 3.5 \times 10^5$ N/m).

respectively. It is observed that in every case, the critical hunting speed increases monotonically with an increasing value of K_{sx}. Moreover, the critical hunting speeds obtained via the linear creep model are consistently higher than those derived from the nonlinear creep model. In addition, for both creep models, the critical hunting speeds obtained from the 6-DOF and 14-DOF systems are higher than those obtained from the 20-DOF system.

In general, Figs. 5–9 show that when the stability analysis is performed utilizing the nonlinear creep model, the critical hunting speeds evaluated via the 14-DOF system are generally higher than those evaluated via the 20-DOF system. Thus, it can be concluded that the critical hunting speed of a railway vehicle moving on curved tracks may be over estimated if the vertical displacements and roll angles of the truck frames and car body are not taken into account.

As discussed at the beginning of this section, neither the vertical stiffness nor the vertical damping of the secondary suspension is considered in the 6-DOF and 14-DOF dynamic system models. A review of the available literature reveals that the influences of these two physical parameters on the critical hunting speed of HSR vehicles during curving have not been fully considered. Accordingly, Fig. 10(a) illustrates the effect of the vertical stiffness of the secondary suspension, K_{sz}, on the critical hunting speed as evaluated via the linear and nonlinear creep models based on the 20-DOF dynamic system. (Note that the track is assumed to have a radius of 6250 m in both cases.) The results show that for both creep models, the critical hunting speed decreases initially with increasing K_{sz} and then increases. In addition, it is observed that the critical hunting speed evaluated via the linear creep model is consistently higher than that obtained from the nonlinear creep model. Fig. 10(b) shows that for a given value of K_{sz}, the critical hunting speed increases with an increasing track radius. (Note that the results are obtained using the nonlinear creep model.).

Fig. 11 illustrates the effect of the vertical damping of the secondary suspension, C_{sz}, on the critical hunting speed of the railway vehicle. (Note that the track is assumed to have a radius of 6250 m in both cases.) It is observed that the critical hunting speed increases with an increasing value of C_{sz} irrespective of the creep model applied. It is also noted that the critical hunting speed evaluated via the linear creep model is generally higher than that obtained from the nonlinear creep model. However, for low values of C_{sz}, the difference in the results obtained from the two creep models is very small. Fig. 11(b) shows that for a given value of C_{sz}, the critical hunting speed increases with an increasing track radius. In addition, it is observed that for a track radius greater than 6250 m, the critical hunting speed reduces with an increasing value of C_{sz}.

5. Conclusions

This study has utilized a heuristic nonlinear creep model to analyze the dynamic behavior of a high-speed railway vehicle during curving. The dynamics of the railway vehicle have been fully described utilizing a 21-DOF model comprising the lateral displacement and yaw angle of each wheelset, the lateral displacement, vertical displacement, roll angle and yaw angle of the truck frame, and the lateral displacement, vertical displacement, roll angle, pitch angle and yaw angle of the car body. The effects of the major system parameters on the hunting stability of the railway vehicle have been examined utilizing reduced dynamic models with 6-, 14- and 20-DOF, respectively. The 20-DOF model is obtained by excluding the nodding motion of the car body (i.e. the pitch angle) from the 21-DOF model, while the 6-DOF and 14-DOF models are obtained by excluding further system parameters from the full model, most notably those relating to the vertical stiffness and vertical damping of the secondary suspension. The respective effects of the various physical parameters on the critical hunting speed of the railway vehicle have been analyzed using the Lyapunov indirect method presented in Ref. [15]. The validity of the analytical modeling approach and the numerical solution procedure has been compared by comparing the results obtained using the 6-DOF dynamic model for the critical speed of a railway vehicle traveling on a straight track with the results presented in the literature [19].

Overall, the results have shown that in the majority of cases, the critical hunting speeds evaluated for the railway vehicle during curving via the 6-DOF and 14-DOF dynamic models are higher than those obtained from the 20-DOF model. In addition, the critical hunting speeds obtained using the heuristic nonlinear creep model are generally lower than those obtained from Kalker's linear creep model [16]. Comparing the results obtained from the 14-DOF model and the 20-DOF model, respectively, it has been shown that the critical hunting speed evaluated via the nonlinear creep model may be over estimated if the vertical displacements and roll angles of the truck frame and car body are not considered. The results obtained using the 20-DOF model have shown that the critical hunting speed first decreases and then increases with an increasing vertical stiffness of the secondary suspension K_{sz}. By contrast, the critical hunting speed increases continuously with an increasing vertical damping of the secondary suspension, C_{sz}, provided that the track radius does not exceed a value of $R = 6250$ m. Finally, for constant values of K_{sz} and C_{sz}, the critical hunting speed increases with an increasing curve radius.

Acknowledgment

The authors gratefully acknowledge the financial support provided to this study by the National Science Council of Taiwan, ROC, under Grant no. NSC96-2218-E-327-030.

Appendix A. System parameters [20,21]

Parameters	Value
Wheelset mass	$m_w = 1117.9\,\mathrm{kg}$
Bogie frame mass	$m_t = 350.26\,\mathrm{kg}$
Car body mass	$m_c = 8041.3\,\mathrm{kg}$
Roll moment of inertia of wheelset	$I_{wx} = 608.1\,\mathrm{kg\,m^2}$
Spin moment of inertia of wheelset	$I_{wy} = 72\,\mathrm{kg\,m^2}$
Yaw moment of inertia of wheelset	$I_{wz} = 608.1\,\mathrm{kg\,m^2}$
Roll moment of inertia of bogie frame	$I_{tx} = 300\,\mathrm{kg\,m^2}$
Yaw moment of inertia of bogie frame	$I_{tz} = 105.2\,\mathrm{kg\,m^2}$
Roll moment of inertia of car body	$I_{cx} = 14\,270\,\mathrm{kg\,m^2}$
Yaw moment of inertia of car body	$I_{cz} = 123\,760.5\,\mathrm{kg\,m^2}$
Wheel radius	$r_0 = 0.43\,\mathrm{m}$
Half of track gauge	$a = 0.7175\,\mathrm{m}$
Wheel conicity	$\lambda = 0.05$
Half of primary longitudinal spring arm	$b_1 = 1.0\,\mathrm{m}$
Half of primary longitudinal damping arm	$b_1 = 1.0\,\mathrm{m}$
Half of primary vertical spring arm	$b_1 = 1.0\,\mathrm{m}$
Half of primary vertical damping arm	$b_1 = 1.0\,\mathrm{m}$
Half of secondary longitudinal spring arm	$b_2 = 1.18\,\mathrm{m}$
Half of secondary longitudinal damping arm	$b_3 = 1.4\,\mathrm{m}$
Half of secondary vertical spring arm	$b_2 = 1.18\,\mathrm{m}$
Half of secondary vertical damping arm	$b_3 = 1.4\,\mathrm{m}$
Half of primary lateral spring arm	$L_1 = 1.28\,\mathrm{m}$
Half of primary lateral damping arm	$L_2 = 1.5\,\mathrm{m}$
Longitudinal distance from wheelset center of gravity to car body	$L_c = 4.2\,\mathrm{m}$
Vertical distance from wheelset center of gravity to secondary suspension	$h_T = 0.47\,\mathrm{m}$
Longitudinal stiffness of primary suspension	$K_{px} = 9 \times 10^5\,\mathrm{N/m}$
Lateral stiffness of primary suspension	$K_{py} = 3.9 \times 10^5\,\mathrm{N/m}$
Vertical stiffness of primary suspension	$K_{pz} = 6 \times 10^5\,\mathrm{N/m}$
Vertical damping of primary suspension	$C_{pz} = 4 \times 10^4\,\mathrm{N\,s/m}$
Longitudinal stiffness of secondary suspension	$K_{sx} = 3.5 \times 10^4\,\mathrm{N/m}$
Lateral stiffness of secondary suspension	$K_{sy} = 3.5 \times 10^4\,\mathrm{N/m}$
Vertical stiffness of secondary suspension	$K_{sz} = 3.5 \times 10^5\,\mathrm{N/m}$
Longitudinal damping of secondary suspension	$C_{sx} = 3.2 \times 10^4\,\mathrm{N\,s/m}$
Lateral damping of secondary suspension	$C_{sy} = 1 \times 10^4\,\mathrm{N\,s/m}$
Vertical damping of secondary suspension	$C_{sz} = 4 \times 10^4\,\mathrm{N\,s/m}$
Lateral rail stiffness	$K_r = 1.617 \times 10^7\,\mathrm{N/m}$
Flange clearance	$\delta = 0.00923\,\mathrm{m}$
Lateral creep force coefficient	$f_{11} = 2.212 \times 10^6\,\mathrm{N}$
Lateral/spin creep force coefficient	$f_{12} = 3120\,\mathrm{N\,m^2}$

Spin creep force coefficient	$f_{22} = 16\,\mathrm{N}$
Longitudinal creep force coefficient	$f_{33} = 2.563 \times 10^6\,\mathrm{N}$
Radius of curved tracks	$R = 6250\,\mathrm{m}$
Superelevation angle of curved track	$\phi_{se} = 0.0873\,\mathrm{rad}$
Axle load	$W = 5.6 \times 10^4\,\mathrm{N}$
Coefficient of friction	$\mu = 0.2$
Normal force acting on wheelset in equilibrium state	$N = W/2\,\mathrm{N}$

References

[1] R.V. Dukkipati, S.S. Narayana, Lateral stability and steady state curving performance of unconventional rail trucks, *Mechanism and Machine Theory* 36 (2001) 577–587.

[2] R.V. Dukkipati, S.S. Narayana, M.O.M. Osman, Curving analysis of modified designs of passenger railway vehicle trucks, *JSME International Journal, Series C: Mechanical Systems, Machine Elements and Manufacturing* 25 (1) (2002) 159–167.

[3] S.Y. Lee, Y.C. Cheng, Influences of the vertical and the roll motions of frames on the hunting stability of trucks moving on curved tracks, *Journal of Sound and Vibration* 294 (2006) 441–453.

[4] S.Y. Lee, Y.C. Cheng, Nonlinear analysis on the hunting stability of high-speed railway vehicle trucks on curved tracks, *Transactions of the ASME Journal of Vibrations and Acoustics* 127 (4) (2005) 324–332.

[5] Y. Suda, High speed stability and curving performance of longitudinally unsymmetric trucks with semi-active control, *Vehicle Systems Dynamics* 23 (1994) 29–51.

[6] C.E. Bell, D. Horak, J.K. Hedrick, Stability and curving mechanics of rail vehicles, *Transaction of the ASME, Journal of Dynamic, Systems, Measurement and Control* 103 (1981) 181–190.

[7] A.K.W. Ahmed, C. Liu, I. Haque, Computer simulation of steady state curving performance of high speed articulated train set, *Transactions of CSME* 20 (1996) 365–389.

[8] A.H. Wickens, Railway vehicles with generic bogies capable of perfect steering, *Vehicle System Dynamics* 25 (1996) 389–412.

[9] C.E. Bell, D. Horak, Forced steering of rail vehicles: stability and curving mechanics, *Vehicle Systems Dynamics* 10 (1981) 357–386.

[10] K. Zboinski, Dynamical investigation of railway vehicles on a curved track, *European Journal of Mechanics A: Solids* 17 (6) (1998) 1001–1020.

[11] K. Zboinski, Importance of imaginary forces and kinematic type non-linearities for description of railway vehicle dynamics, *Proceeding of the IMECHE Part F, Journal of Rail and Rapid Transit* 213 (4) (1999) 199–210.

[12] J. Zeng, P. Wu, Stability analysis of high speed railway vehicles, *JSME International Journal, Series C: Mechanical Systems, Machine Elements and Manufacturing* 47 (2) (2004) 464–470.

[13] T. Hirotsu, F. Iwasaki, K. Terada, M. Ariga, Curving simulation of four axle railway vehicles with conventional two axle bogie, *Bulletin of JSME* 27 (228) (1984) 1272–1279.

[14] K. Zboinski, M. Dusza, Analysis and method of the analysis of non-linear lateral stability of railway vehicles in curved track, *Vehicle System Dynamics* 41 (supplement) (2004) 222–231.

[15] M. Vidyasager, *Nonlinear Systems Analysis*, Prentice-Hall, Englewood Cliffs, NJ, 1978.

[16] R.V. Dukkipati, V.K. Garg, *Dynamics of Railway Vehicle Systems*, Academic Press, Canada, 1984.

[17] D. Horak, D.N. Wormley, Nonlinear stability and tracking of rail passenger trucks, *ASME Journal of Dynamic Systems, Measurement, and Control* 104 (1982) 256–263.

[18] S. Iwnicki, *Handbook of Railway Vehicle Dynamics*, Taylor & Francis, London, 2006.

[19] M. Ahmadian, S. Yang, Effect of system nonlinearities on locomotive bogie hunting stability, *Vehicle System Dynamics* 29 (1998) 366–384.

[20] A.K.W. Ahmed, S. Sankar, Lateral stability behavior of railway freight car system with elasto-damper coupled wheelset: part 2—truck model, *Transactions of the ASME, Journal of Mechanisms, Transmissions, and Automation in Design* 109 (4) (1987) 500–507.

[21] T. Hirotsu, K. Terada, M. Hiraishi, S. Yui, Simulation of hunting of rail vehicles (the case using a compound circular wheel profile), *JSME International Journal Series III, Vibration, Control Engineering, Engineering for Industry* 34 (3) (1991) 396–403.